

Effect of Cross-Section Shape on Seismic Behavior of Moment Frames with CFT Columns under Near- and Far-Field Earthquakes

Mahdian pari J.¹, Farahbod F.², Faroughi A.³.

Abstract:

This study examines the effect of cross-sectional shape on the nonlinear seismic behavior of Concrete-Filled Tube (CFT) columns in moment-resisting steel frames subjected to near- and far-field earthquakes. Two-dimensional frames with varying heights were modeled using finite element analysis in ABAQUS, incorporating square, circular, and rectangular CFT columns. Nonlinear dynamic analysis was performed to evaluate seismic performance in terms of displacement, base shear, inter-story drift, and bending moment. Results show that circular CFT columns outperform others in low-rise frames, exhibiting up to 27% lower displacement and reduced drift under far-field earthquakes. In contrast, rectangular CFT columns demonstrate superior performance in mid- to high-rise frames, with up to 59% less displacement and 44% lower base shear under both near- and far-field conditions. Square sections consistently exhibited the poorest performance. Far-field earthquakes induced higher responses, with an average increase of 27-34% in bending moment. These findings underscore the critical influence of cross-sectional shape on optimizing the seismic design of CFT columns in moment frames for earthquake-prone regions.

Keywords: Concrete-Filled Tube (CFT), Seismic Behavior, Moment-Resisting Frames, Cross-Section Shape, Finite Element Method.

✉*Corresponding author Email: javad.mahdianpari@iau.ac.ir

1 * Ph.D. Candidate, Department of Civil Engineering, WT.C., Islamic Azad University, Tehran, Iran

2 Assistant Professor, Department of Civil Engineering, WT.C., Islamic Azad University, Tehran, Iran

3 Assistant Professor, Department of Civil Engineering, ET.C., Islamic Azad University, Tehran, Iran

1. Introduction

Concrete-Filled Tube (CFT) columns are widely utilized in earthquake-resistant structures due to their combined advantages of steel and concrete, including high strength, ductility, and energy dissipation capacity. These columns consist of an external steel tube filled with concrete, with their composite behavior under seismic loading enhanced by the confinement effect of the steel tube on the concrete core [1]. Steel moment-resisting frames incorporating CFT columns are ideal for high-rise structures in seismic-prone regions due to their significant stiffness and strength [2]. However, the seismic behavior of CFT columns under near- and far-field earthquakes, particularly with varying cross-sectional shapes (square, circular, and rectangular), requires further investigation [3].

Near-field earthquakes, characterized by high-velocity pulses and high acceleration, and far-field earthquakes, with longer durations and lower frequency content, impose distinct effects on the structural response of CFT columns [4]. The cross-sectional shape of the column significantly influences stress distribution and ductility capacity; for instance, circular sections typically provide better confinement compared to square sections [5]. Moreover, nonlinear dynamic analyses using software such as ABAQUS enable precise simulation of the nonlinear material behavior and steel-concrete interactions [6]. Despite recent advancements, the impact of cross-sectional shape and earthquake type on seismic response parameters, such as displacement, base shear, and inter-story drift, remains underexplored [7].

This study aims to investigate the seismic behavior of CFT columns in steel moment-

resisting frames under near- and far-field earthquakes using nonlinear dynamic analysis. Specifically, it focuses on the influence of cross-sectional shape (square, circular, and rectangular) on seismic performance, employing finite element modeling in ABAQUS to simulate structural responses. The findings are expected to contribute to the optimization of seismic design for composite structures [8].

2. Literature Review

Concrete-Filled Tube (CFT) columns have emerged as a promising solution for enhancing the seismic performance of steel moment-resisting frames, combining the compressive strength of concrete with the tensile capacity and confinement of steel tubes [9, 10]. Their ability to provide high stiffness, ductility, and energy dissipation makes them particularly suitable for structures in high-seismic-risk regions. Previous research has explored CFT columns under various loading conditions, including static, cyclic, and dynamic seismic loads, highlighting their role in improving structural resilience and safety [11, 12]. This section reviews the existing literature on CFT columns, composite materials, and seismic analysis techniques, identifying critical gaps addressed by the current study.

The seismic behavior of CFT columns with different cross-sectional shapes—square, circular, and rectangular—has been a focal point of recent studies, particularly under near- and far-field earthquakes. Garmeh et al. [10] developed a self-centering eccentrically braced frame with CFT columns, demonstrating enhanced energy dissipation and reduced residual deformations under seismic loading. Similarly, Hassani et al. [16] analyzed the nonlinear seismic response of CFT columns in tunnel linings, emphasizing their capacity to withstand ground motions.

These studies indicate that circular cross-sections typically offer higher ductility due to uniform confinement, while rectangular cross-sections provide greater axial stiffness, which is advantageous in taller structures [13, 14]. However, comprehensive comparisons of square, circular, and rectangular CFT columns across varying building heights and earthquake types remain limited, a gap the present study seeks to address [12, 15].

Composite materials, such as Fiber-Reinforced Polymer (FRP) and advanced concrete mixtures, have been extensively studied for strengthening and retrofitting structures, with potential applications in CFT columns. Kabir and Hojatkashani [11, 13, 17, 25, 26, 27] conducted experimental and analytical studies on FRP-retrofitted reinforced concrete beams, focusing on interfacial stress distribution and fatigue performance under cyclic loading. Their findings underscore the effectiveness of FRP in enhancing structural capacity and confinement, principles applicable to the steel-concrete interface in CFT columns [23]. Furthermore, Eskandarinia et al. [9] investigated alkali-activated slag-based concrete reinforced with recycled tire steel fibers, reporting improved mechanical properties and sustainability, which could enhance the performance of CFT concrete cores [15, 18]. These advancements highlight the need to explore high-strength and nano-enhanced concrete in CFT designs to optimize seismic performance.

Seismic analysis techniques, including finite element modeling and experimental testing, have been instrumental in understanding the behavior of CFT columns under earthquake loading. Arezoomand Langarudi et al. [21, 28] evaluated the seismic performance of steel plate shear walls, emphasizing the role of design optimality and overstrength, which

are relevant to optimizing CFT column designs in moment-resisting frames. Farokhizadeh et al. [22] studied the effect of fiber addition on the seismic performance of segmental tunnel linings, demonstrating improved ductility and energy absorption, concepts that can be extended to CFT columns [29]. Additionally, Kia Darbandsari and Hojatkashani [14] reviewed structure-soil-structure interaction, highlighting its impact on seismic response in high-rise buildings, a critical consideration for CFT columns [16, 24]. These studies provide a robust foundation for the nonlinear dynamic analyses conducted in the current study using ABAQUS/Explicit.

Despite these advancements, significant gaps remain in the literature. Most studies focus on specific cross-sections or loading conditions, with limited attention to the combined effects of near- and far-field earthquakes on CFT columns in low- to high-rise structures [17, 19, 20]. Furthermore, the integration of advanced composite materials, such as nano-enhanced concrete or high-strength FRP, into CFT columns is underexplored, as is the standardization of design guidelines for different cross-sectional shapes [18, 31]. The current study addresses these gaps by systematically analyzing the seismic behavior of square, circular, and rectangular CFT columns in 3-, 5-, and 8-story frames under near- and far-field earthquakes, providing quantitative insights into displacement, drift, base shear, and bending moment responses. By examining the influence of cross-sectional shape on axial stiffness and ductility, this study contributes to the development of optimized seismic design strategies for composite structures.

3. Methodology

This study investigates the seismic behavior

of Concrete-Filled Tube (CFT) columns in steel moment-resisting frames under near- and far-field earthquakes. The methodology involves the design and numerical modeling of two-dimensional moment-resisting frames, the application of earthquake accelerograms, and the evaluation of structural responses such as maximum displacement, base shear, inter-story drift, and bending moment. Nonlinear dynamic analyses were conducted using the ABAQUS/Explicit software, selected for its capability to simulate the nonlinear behavior of composite materials and the complex interactions between steel and concrete.

3-1- Structural Models

To investigate the influence of cross-sectional shape on seismic performance, two-dimensional steel moment-resisting frames with heights of 3, 5, and 8 stories, representing short, medium, and relatively tall structures, were designed and modeled. Each frame consisted of I-shaped steel beams and CFT columns with square, circular, and rectangular cross-sections, with rigid (moment-resisting) connections to ensure full moment transfer between beams and columns. The dimensions of the column cross-sections were selected based on the AISC 360-16 standard to comply with the seismic design requirements for high-risk regions. Additionally, IPB 24 beams were used for the design and analysis of the studied frames. In each of the models, regardless of the number of stories, the number of bays was fixed at 3 bays. The bay width was selected as 5 meters, and the story height was chosen as 3.2 meters. The material properties included the steel tube with a yield strength of 240 MPa and an elastic modulus of 200 GPa, and the concrete core with a compressive strength of 30 MPa,

which are consistent with common applications in composite structures. The cross-sections used for the columns are presented in Table (1).

Table 1. Cross-sections of columns used in the article

Name of the CFT section	External dimensions of the column	Thickness of the plate
Square-shaped section	40×40 cm	1 cm
Circular section	40 cm	1 cm
Rectangular section	40×25 cm	1 cm

3-2- Finite Element Models

Finite element models were developed in the ABAQUS/Explicit software to accurately capture the nonlinear dynamic response of CFT columns. The steel tube was simulated using shell elements (S4R) with a bilinear stress-strain model (incorporating plastic behavior). The concrete core was modeled using solid elements (C3D8R) with the Concrete Damaged Plasticity (CDP) model, which enables the simulation of cracking and crushing of concrete. The interaction between the steel tube and the concrete core was modeled using a surface-to-surface contact algorithm (with tangential friction and hard normal contact) to simulate composite behavior without slippage.

The element mesh size was calibrated through sensitivity analysis to balance computational accuracy and analysis time. A finer mesh (20 mm) was applied in critical regions of the columns (column base and moment-resisting connections), while a coarser mesh (50 mm) was used in other regions. Gravity loads (dead and live loads) were applied prior to seismic excitation in accordance with the ASCE 7-16 standard to represent realistic initial structural conditions. Figure (1) illustrates an example of the mesh configuration in the models.

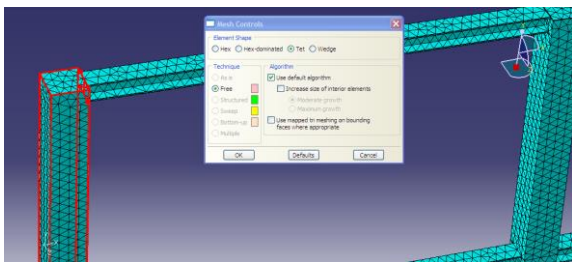


Fig. 1. Final mesh configuration of the model

3-3- Earthquake loading

To evaluate seismic performance, three near-field earthquake accelerograms and three far-field earthquake accelerograms were selected. The accelerograms were scaled using the spectral matching method in accordance with the ASCE 7-16 standard to align with the design spectrum for high-seismic-risk regions. These accelerograms were applied horizontally to the base of the frames to simulate unidirectional seismic excitation. The specifications of the accelerograms, including name, earthquake type, PGA, duration, and frequency content, are presented in Tables (2) and (3).

3-4- Nonlinear Dynamic Analysis

Nonlinear dynamic analyses were conducted to evaluate the seismic response of the frames. The explicit time integration scheme in ABAQUS/Explicit was employed to accurately capture the complex nonlinear interactions between the steel tube and the concrete core under dynamic loading. The key response parameters included the following:

- Maximum displacement at the top story.
- Base shear at the frame's base.
- Maximum inter-story drift.
- Bending moment at critical column sections (column base).

Structural damping was applied using the

Rayleigh damping model with a damping ratio of 5% for the first and second modes. The analysis duration for each accelerogram was adjusted to capture the complete structural response, including post-peak earthquake behavior. The analysis settings, including time step and convergence criteria, were consistent with dynamic analysis standards.

3-5- Model Validation

The finite element models were validated by comparing the predicted responses with experimental data from reputable studies. The focus of the validation was on the load-displacement behavior of the tube under cyclic loading [32]. In this article, a CFT column subjected to biaxial bending was investigated. Figure (2) provides a general overview of the presented model. The presented model is subjected to an axial load N and a lateral load P , which is applied at an angle relative to the column's cross-section. The axial load remains constant, while variations occur in the lateral load. The CCFT2 model was selected for construction and comparison. This model was based on experimental studies, and its experimental setup is presented in Figure (3). The model has the specifications provided in Table (4). Table (4) also includes the specifications of the validation model.

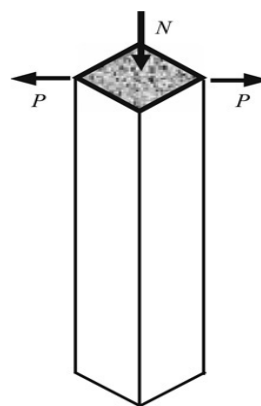


Fig. 2. General overview of the validation model [32].

Table 2. Specifications of the considered near-fault earthquakes

Row	Earthquake	Date of occurrence	Type of soil	Distance from the fault (km)	PGA (m/s ²)	PGV (m/s)	PGD (m)
1	Kocaeli, Turkey	1999/08/17	II	1.38	0.3218	0.71	0.4732
2	Imperial Valley-06	1979/10/15	II	0	0.4490	1.13	0.7288
3	Tabas, Iran	1978/09/16	II	1.79	0.8617	1.23	0.9363

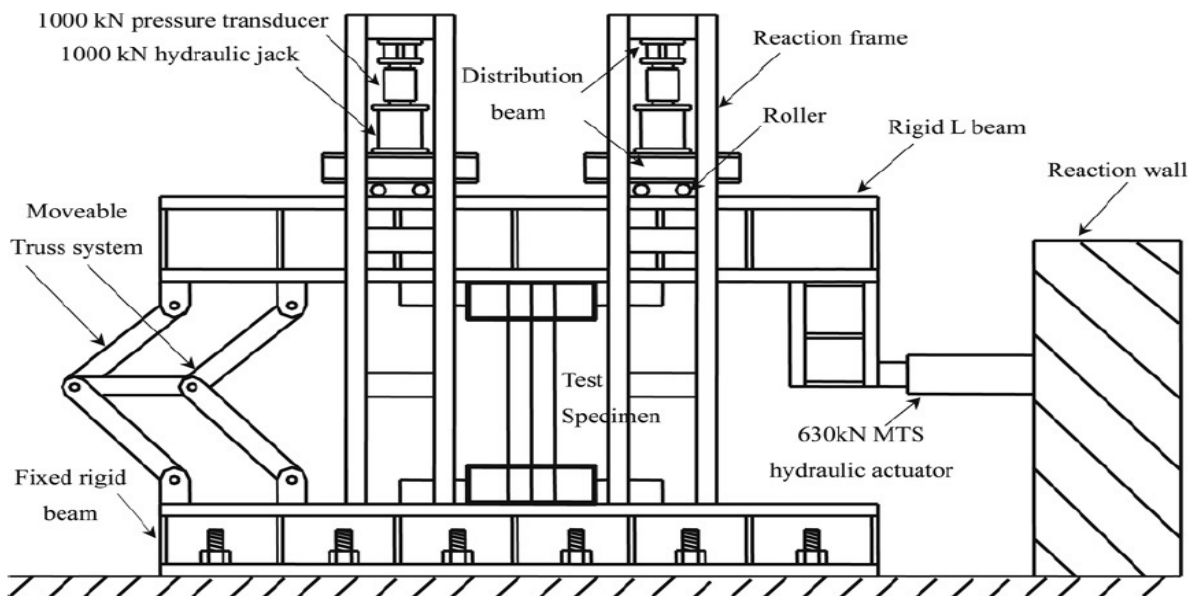
Table 3. Specifications of the considered near-fault earthquakes

Row	Earthquake	Date of occurrence	Type of soil	Distance from the fault (km)	PGA (m/s ²)	PGV (m/s)	PGD (m)
1	Kobe, Japan	1995/01/16	II	95.72	0.1498	0.14	0.0229
2	Imperial Valley-06	1979/10/15	II	19.76	0.1411	0.16	0.0981
3	Northridge	1994/01/17	II	82.01	0.1042	0.76	0.0081

Table 4. Specifications of the validation model [32].

Parameters of test specimens

Specimen	D (mm)	t (mm)	D/t	L (mm)	f_{cu}^{10} (MPa)	f_{co} (MPa)	f_y (MPa)	N (kN)	n_0	θ (°)	P_u (kN)
CCFT1	150	2.65	56.6	1100	48.8	35.2	328	662	0.52	45	80.0
CCFT2	150	2.65	56.6	1100	48.8	35.2	328	452	0.35	45	74.7
CCFT3	150	4.82	31.1	1100	48.8	35.2	340	592	0.35	45	122.5
CCFT4	150	2.65	56.6	845	48.8	35.2	328	452	0.35	45	109.3
CCFT5	150	2.65	56.6	1100	48.8	35.2	328	452	0.35	22.5	78.5
HCFT1	150	4.78	31.4	1100	100.5	81.4	317	1300	0.52	45	164.1
HCFT2	150	2.89	51.9	1100	100.5	81.4	319	1300	0.58	45	125.8
HCFT3	150	2.89	51.9	1100	100.5	81.4	319	1000	0.45	45	130.4
HCFT4	150	2.89	51.9	800	100.5	81.4	319	1000	0.45	45	160.4

**Fig. 3. Experimental setup of the validation model [32].**

In this article, load-displacement curves are presented for various conditions of confined concrete types and different column plate thicknesses. The graph showing the variation of mid-column lateral displacement against changes in lateral force is illustrated in Figure (4) for the CCFT2 sample. The results demonstrated that the ABAQUS models

simulate the nonlinear behavior of CFT columns with an error of less than 10% compared to experimental data. This validation process ensured confidence in the results of the seismic analyses. The predicted and experimental load-displacement curves are presented in Figure (5).

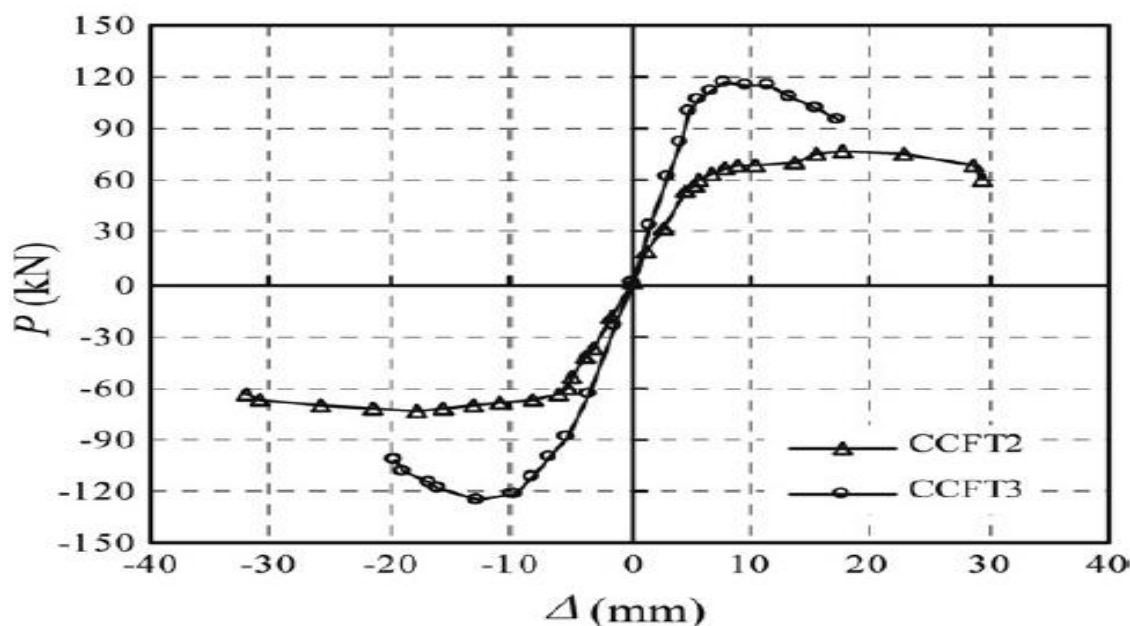


Fig. 4. Force-displacement graph of the experimental model from reference article [32].

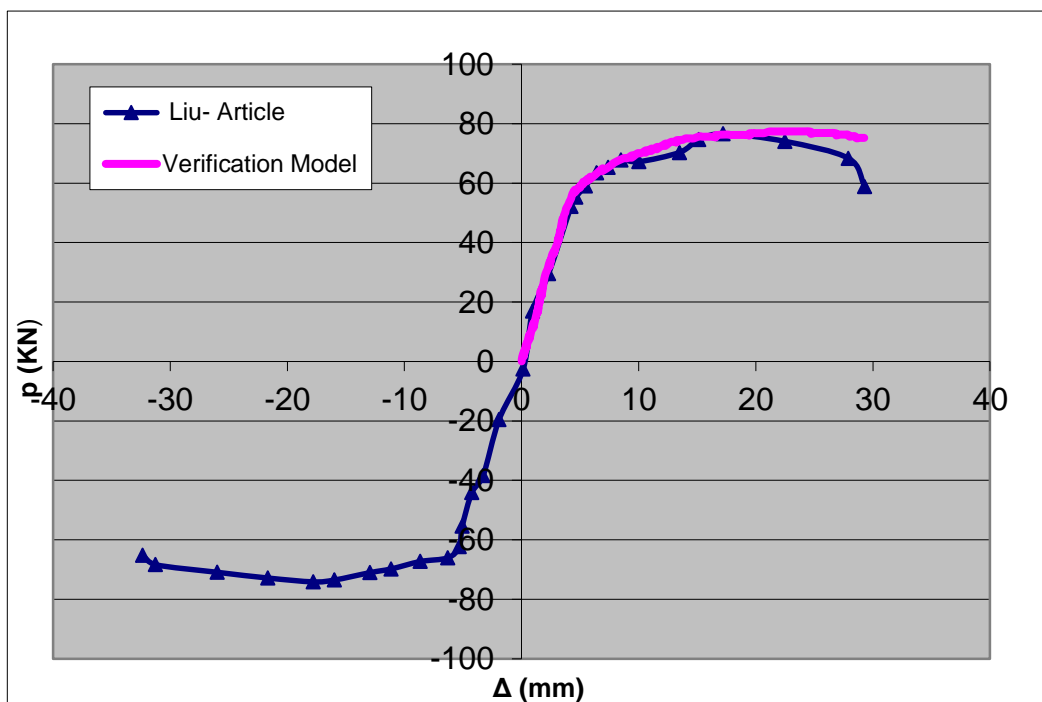


Fig. 5. Comparison of load-displacement curves of the experimental and software models.

4. Results and Discussion

In this article, the seismic behavior of Concrete-Filled Tube (CFT) columns with three types of cross-sections (square, circular, and rectangular) in steel moment-resisting frames with heights of 3, 5, and 8 stories was analyzed under near- and far-field earthquakes. Nonlinear dynamic analyses were performed using the ABAQUS/Explicit software to evaluate key structural responses, including maximum displacement, inter-story drift, base shear, and bending moment. As an

example, the deformation of three modeled frames with rectangular cross-sections under one of the near-field earthquakes (Tabas earthquake) is presented in Figure (6). Due to the large number of models, the inclusion of images for all models has been avoided. The analysis results are presented in the tables and figures below to provide a precise comparison of the performance of different cross-sections, number of stories, and earthquake types.

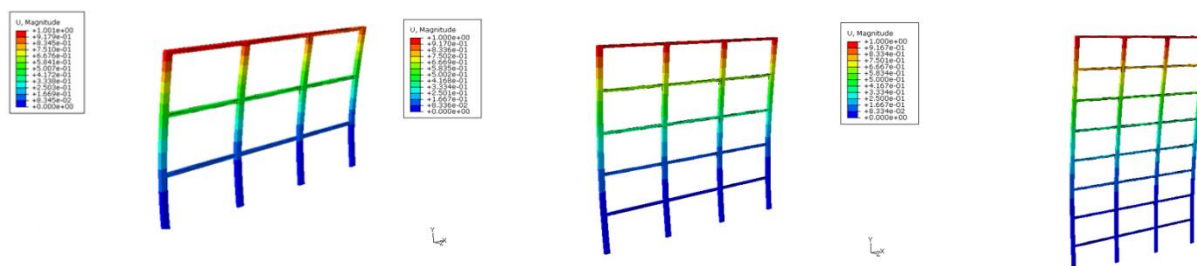


Fig. 6. Deformation of the 3, 5, and 8-story models under the Tabas earthquake (near-field).

4-1- Maximum Displacement Results

The maximum displacement at the top level of the 3, 5, and 8-story models with square, circular, and rectangular cross-sections was investigated under near- and far-field earthquakes. The results are summarized in Table (5), and comparative charts are presented in Figures (7) to (9).

- **3-Story Models:**

Based on the comparison of the top-level displacement of the 3-story model for different cross-sections under far-field earthquake records, it was observed that the circular cross-section exhibited less displacement under similar conditions compared to the rectangular and square cross-sections. In this case, the circular cross-section showed 27% less displacement less than that of the square cross-section. Under far-field earthquakes, the

compared to the square cross-section and 45% less compared to the rectangular cross-section. Under near-field earthquakes, the performance of all three cross-section types was nearly identical, with the circular cross-section exhibiting the least displacement.

- **5-Story Models:**

Based on the comparison of the top-level displacement of the 5-story model for different cross-sections under near- and far-field earthquake records, it was observed that the rectangular cross-section exhibited less displacement under similar conditions compared to the circular and square cross-sections. This holds true for both near- and far-field earthquakes. Under near-field earthquakes, the displacement for the rectangular cross-section was 34% less than that of the circular cross-section and 45% displacement for the rectangular cross-section was 53% less than that of the circular

cross-section and 58% less than that of the square cross-section.

- **8-Story Models:**

Based on the comparison chart of the top-level displacement of the 8-story model for different cross-sections under near- and far-field earthquake records, it was observed that the highest displacement values for both near- and far-field earthquakes occurred for the square cross-section columns. Additionally, the lowest displacement values were observed in frames with rectangular cross-sections. Under near-field earthquakes, the rectangular cross-section experienced

11% less displacement compared to the circular cross-section and 19% less compared to the square cross-section. Furthermore, under far-field earthquakes, the rectangular cross-section showed 47% and 59% less displacement compared to the circular and square cross-sections, respectively. Overall, displacement values under far-field earthquakes were higher than those caused by near-field earthquakes, with an average increase of 29%.

Table 5. Maximum displacement of the investigated models (cm)

Specifications		Near-Field earthquake			Far-field earthquake		
Stories	Type of Column	Tabas	Imperial Valley	Kocaeli	Northridge	Imperial Valley	Kobe
Three-story	Square cross-section	4.7	4.2	4.1	8.9	8.0	7.8
	Circular cross-section	4.5	4.0	3.9	6.5	5.8	5.7
	Rectangular cross-section	4.6	4.0	4.1	11.8	10.4	10.5
Five-story	Square cross-section	17.8	16.2	16.0	35.1	31.9	31.6
	Circular cross-section	15	13.8	13.7	31.1	28.6	28.3
	Rectangular cross-section	9.8	8.8	8.6	14.6	13.1	12.8
Eight-story	Square cross-section	21.1	18.8	19.0	37	32.9	33.3
	Circular cross-section	19.2	17.7	16.7	29.2	26.9	25.4
	Rectangular cross-section	17	15.8	15.3	15.2	14.1	13.7

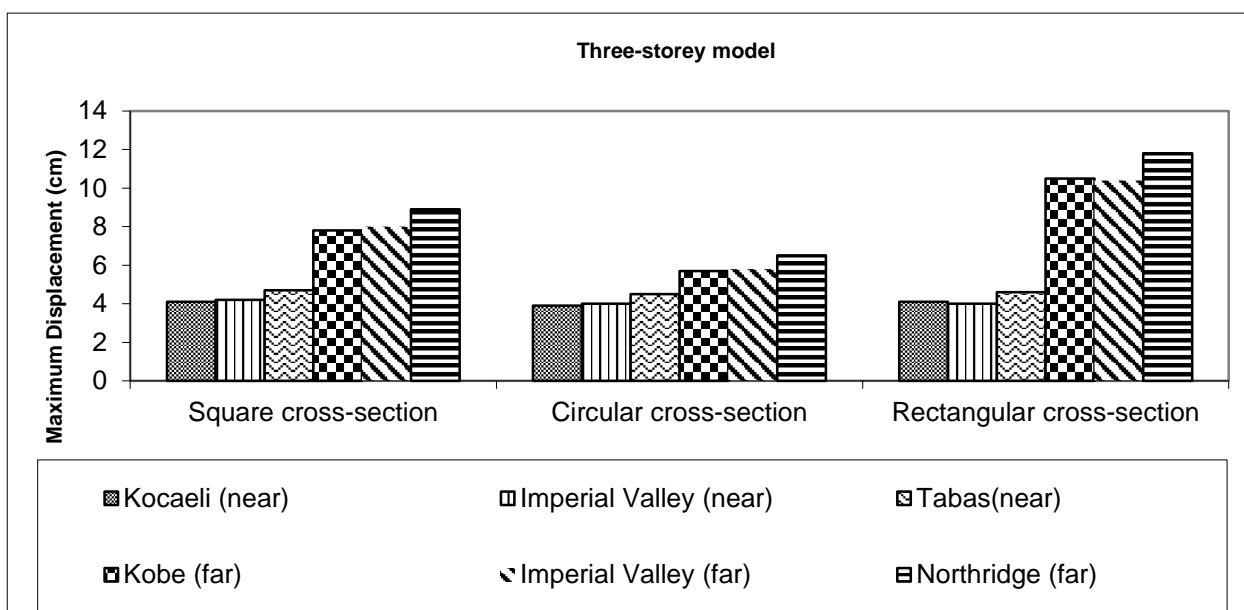


Fig. 7. Comparison of maximum displacement in three-story CFT models under different earthquakes.

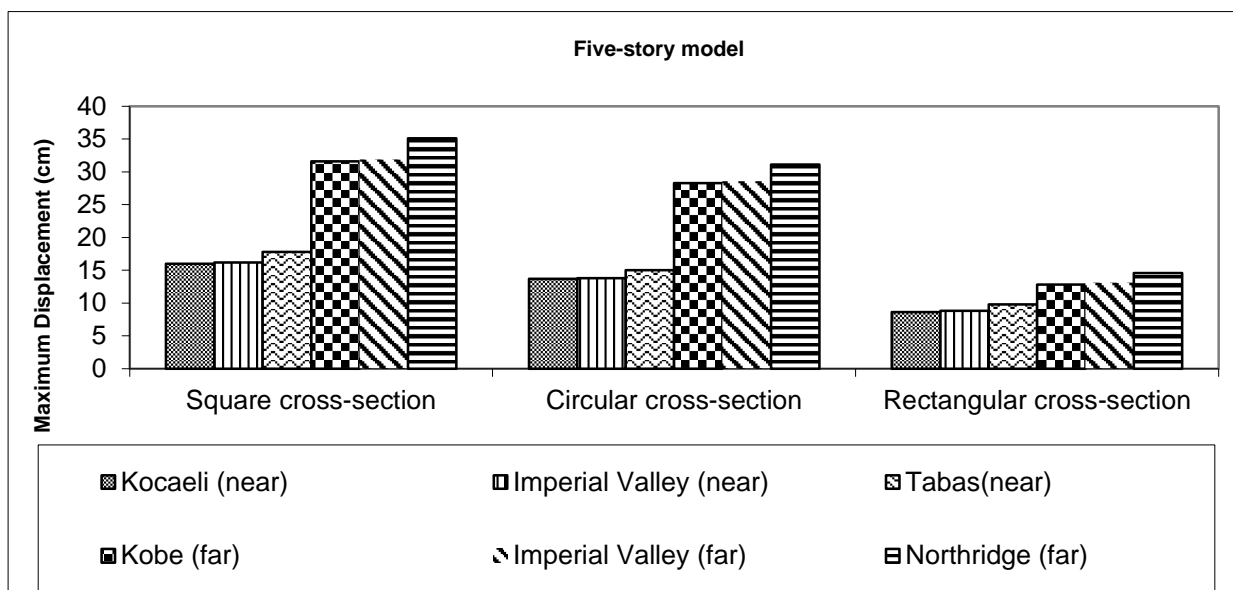


Fig. 8. Comparison of maximum displacement in Five-story CFT models under different earthquakes.

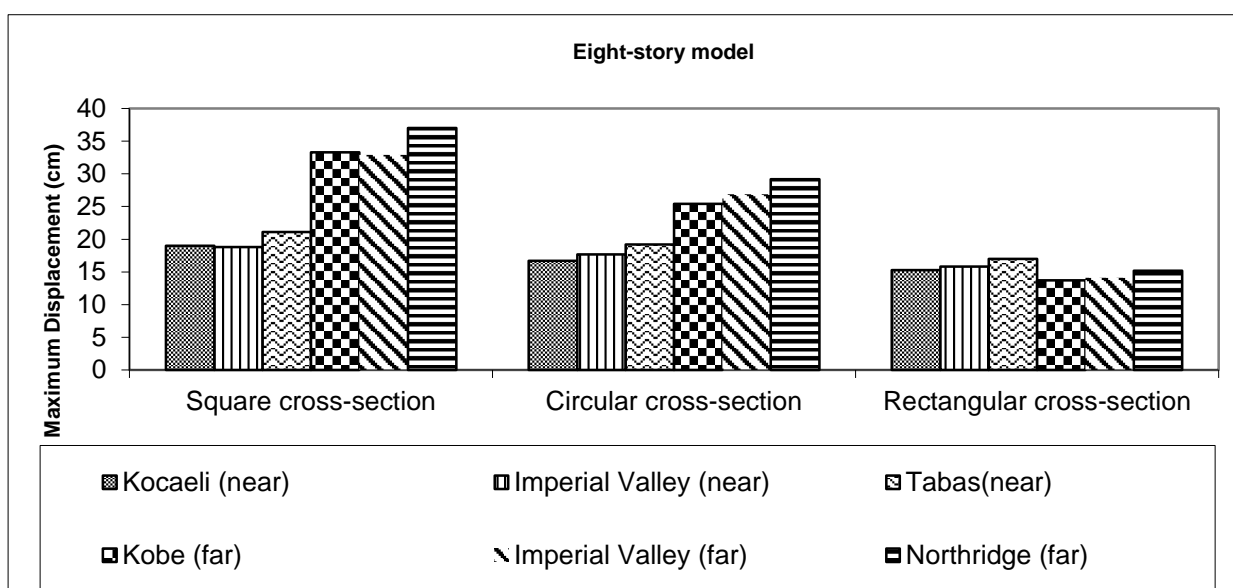


Fig. 9. Comparison of maximum displacement in Eight-story CFT models under different earthquakes.

4-2- Inter-Story Drift Results

The maximum inter-story drift for the 3, 5, and 8-story models under near- and far-field earthquakes was investigated. The results are summarized in Table (6).

Three-story models

According to the maximum drift diagrams for the three-storey building under near-fault earthquakes, the lowest drift values were approximately observed in the model with

rectangular column sections. Overall, the three types of column sections exhibited similar behavior in the three-storey models. Under far-fault earthquakes, the lowest drift was approximately recorded in the model with circular column sections.

- **Five-story models:**

Based on the drift diagrams for the five-storey building under near-fault earthquakes, the

rectangular column section demonstrated the lowest drift, while the square section showed the highest drift, indicating poorer performance. Under far-fault conditions, rectangular column sections again showed the lowest drift and the best overall seismic performance.

- **Eight-story models:**

According to the maximum drift results for the

eight-storey model under near-fault earthquakes, rectangular column sections provided the best performance and lowest drift, while square columns showed weaker performance. Under far-fault earthquakes, the lowest drift values in the eight-storey models were also observed in the structures with rectangular column sections.

Table 6. Maximum drift of the studied models

Specifications		Near-Field earthquake			Far-field earthquake		
Stories	Type of Column	Tabas	Imperial Valley	Kocaeli	Northridge	Imperial Valley	Kobe
Three-story	Square cross-section	0.006875	0.00238	0.00245	0.01125	0.00950	0.00980
	Circular cross-section	0.005938	0.00270	0.00273	0.008438	0.00510	0.00515
	Rectangular cross-section	0.005938	0.00364	0.00368	0.015938	0.01000	0.01011
Five-story	Square cross-section	0.01625	0.00796	0.00788	0.02875	0.01746	0.01728
	Circular cross-section	0.012813	0.00480	0.00475	0.034063	0.01590	0.01573
	Rectangular cross-section	0.007188	0.00570	0.00564	0.015625	0.01080	0.01069
Eight-story	Square cross-section	0.010313	0.00849	0.00840	0.020625	0.01122	0.01110
	Circular cross-section	0.009688	0.00911	0.00911	0.013125	0.00852	0.00852
	Rectangular cross-section	0.007813	0.00750	0.00734	0.009063	0.00330	0.00323

4-3- Base Shear Results

The base shear for the 3, 5, and 8-story models under near- and far-field earthquakes was investigated. The results are summarized in Table (7).

- **3-Story Models:**

Based on the comparison of base shear for the 3-story model with different cross-sections under near- and far-field earthquake records, it was observed that the rectangular cross-section exhibited lower base shear under similar conditions compared to the circular and square cross-sections. This holds true for both near- and far-field earthquakes. Under near-field earthquakes, the base shear for the rectangular cross-section was 4% lower than that of the circular cross-section and 10% lower than that of the square cross-section. Under far-field earthquakes, the base shear for the rectangular cross-section was 19% lower than that of the circular cross-section and 26% lower than that of the square

cross-section.

- **5-Story Models:**

Based on the comparison of base shear for the 5-story model with different cross-sections under near- and far-field earthquake records, it was observed that the rectangular cross-section exhibited lower base shear under similar conditions compared to the circular and square cross-sections. This holds true for both near- and far-field earthquakes. Under near-field earthquakes, the base shear for the rectangular cross-section was 11% lower than that of the circular cross-section and 44% lower than that of the square cross-section. Under far-field earthquakes, the base shear for the rectangular cross-section was 15% lower than that of the circular cross-section and 34% lower than that of the square cross-section.

- **8-Story Models:**

Based on the comparison chart of base shear for the 8-story model with different cross-

sections under near- and far-field earthquake records, it was observed that the base shear values for far-field earthquakes were higher than those recorded for near-field earthquakes, with an average increase of 31%. Under near-field earthquakes, the base shear for the circular cross-section was 10%

lower than that of the rectangular cross-section and 31% lower than that of the square cross-section. Under far-field earthquakes, the base shear for the rectangular cross-section was 14% lower than that of the circular cross-section and 28% lower than that of the square cross-section.

Table 7. Base shear of the studied models (ton)

Specifications		Near-Field earthquake			Far-field earthquake		
Stories	Type of Column	Tabas	Imperial Valley	Kocaeli	Northridge	Imperial Valley	Kobe
Three-story	Square cross-section	33	29.7	29.0	49	44.1	43.1
	Circular cross-section	31	27.6	27.0	44.5	39.6	38.7
	Rectangular cross-section	29.6	26.0	26.3	36	31.7	32.0
Five-story	Square cross-section	85.1	77.4	76.6	116	105.6	104.4
	Circular cross-section	53.5	49.2	48.7	90	82.8	81.9
	Rectangular cross-section	47.6	42.8	41.9	76	68.4	66.9
Eight-story	Square cross-section	88	78.3	79.2	126	112.1	113.4
	Circular cross-section	63.3	58.2	55.1	106	97.5	92.2
	Rectangular cross-section	70.6	65.7	63.5	90.9	84.5	81.8

4-4- Bending Moment Results

The bending moment for the 3, 5, and 8-story models under near- and far-field earthquakes was investigated. The results are summarized in Table (8).

• 3-Story Models:

Based on the comparison chart of bending moment for the 3-story model with different cross-sections under near- and far-field earthquake records, it was observed that the bending moment values for far-field earthquakes were higher than those recorded for near-field earthquakes, with an average increase of 27%. Under near-field earthquakes, the bending moment for the rectangular cross-section was 4% lower than that of the circular cross-section and 10% lower than that of the square cross-section. Under far-field earthquakes, the bending moment for the rectangular cross-section was 19% lower than that of the circular cross-section and 26% lower than that of the square cross-section.

• 5-Story Models:

Based on the comparison chart of bending moment for the 5-story model with different cross-sections under near- and far-field earthquake records, it was observed that the bending moment values for far-field earthquakes were higher than those recorded for near-field earthquakes, with an average increase of 34%. Under near-field earthquakes, the bending moment for the rectangular cross-section was 10% lower than that of the circular cross-section and 44% lower than that of the square cross-section. Under far-field earthquakes, the bending moment for the rectangular cross-section was 15% lower than that of the circular cross-section and 34% lower than that of the square cross-section.

• 8-Story Models:

Based on the comparison chart of bending moment for the 8-story model with different cross-sections under near- and far-field earthquake records, it was observed that the bending moment values for far-field

earthquakes were higher than those recorded for near-field earthquakes, with an average increase of 11%. Under near-field earthquakes, the bending moment for the rectangular cross-section was 11% lower than that of the circular cross-section and

27% lower than that of the square cross-section. Under far-field earthquakes, the bending moment for the rectangular cross-section was 14% lower than that of the circular cross-section and 27% lower than that of the square cross-section.

Table 8. Bending moment of the studied models (ton.m)

Specifications		Near-Field earthquake			Far-field earthquake		
Stories	Type of Column	Tabas	Imperial Valley	Kocaeli	Northridge	Imperial Valley	Kobe
Three-story	Square cross-section	297	267.3	261	441	396.9	387.9
	Circular cross-section	279	248.4	243	400.5	356.4	348.3
	Rectangular cross-section	266.4	234	236.7	324	285.3	288
Five-story	Square cross-section	1276.5	1161	1149	1740	1584	1566
	Circular cross-section	802.5	738	730.5	1350	1242	1228.5
	Rectangular cross-section	714	642	628.5	1140	1026	1003.5
Eight-story	Square cross-section	2112	1879.2	1900.8	3024	2690.4	2721.6
	Circular cross-section	1519.2	1396.8	1322.4	2544	2340	2212.8
	Rectangular cross-section	1694.4	1576.8	1524	2181.6	2028	1963.2

5. conclusion

This study investigated the seismic behavior of Concrete-Filled Tube (CFT) columns with square, circular, and rectangular cross-sections in steel moment-resisting frames with heights of 3, 5, and 8 stories under near- and far-field earthquakes. Nonlinear dynamic analyses were performed using ABAQUS/Explicit software to evaluate key structural responses, including maximum displacement, inter-story drift, base shear, and bending moment. The results highlight the significant influence of cross-section shape, number of stories, and earthquake type on the seismic performance of composite structures, providing valuable insights for designing safer structures in high-seismic-risk regions.

The findings revealed that the shape of the CFT column cross-section plays a critical role in seismic response. Rectangular cross-sections generally exhibited superior performance in reducing displacement, drift, base shear, and bending moment compared

to circular and square cross-sections, particularly in medium- to high-rise structures (5 and 8 stories). For instance, in the 8-story model under far-field earthquakes, the rectangular cross-section reduced displacement by 47% and 59% compared to circular and square cross-sections, respectively. Similarly, in the 5-story model, the base shear for the rectangular cross-section under near-field earthquakes was 11% lower than that of the circular cross-section and 44% lower than that of the square cross-section. However, circular cross-sections outperformed others in short structures (3 stories) under far-field earthquakes, showing 27% less displacement than square and 45% less than rectangular cross-sections. Square cross-sections consistently demonstrated the weakest performance, especially in taller structures, likely due to stress concentration at corners and lower confinement capacity.

The number of stories and earthquake type

also significantly influenced structural behavior. Increasing the height from 3 to 8 stories led to a notable increase in displacement and drift, particularly under near-field earthquakes (e.g., the Tabas earthquake), where pulse-like characteristics amplified drift. Conversely, far-field earthquakes, due to their longer duration, induced higher base shear and bending moment. For example, the bending moment under far-field earthquakes was, on average, 27% (3-story), 34% (5-story), and 11% (8-story) higher than under near-field earthquakes. These differences underscore the importance of considering earthquake characteristics in the design of composite structures.

From a seismic design perspective, this study emphasizes the importance of selecting an appropriate cross-section shape. Rectangular cross-sections, with their higher stiffness, better stress distribution, and enhanced confinement capacity, are particularly suitable for medium- to high-rise structures in seismic-prone areas. However, circular cross-sections may be preferable for shorter structures under far-field earthquakes due to their ductility and ability to reduce displacement. Square cross-sections, given their poorer performance, especially in taller buildings, are less recommended. These findings can assist engineers in optimizing

the design of composite structures with CFT columns, thereby enhancing seismic safety.

To further advance this research, future studies are recommended to focus on the following areas: 1) investigating the seismic behavior of CFT columns with unconventional cross-sections, such as polygonal or elliptical shapes, for comparison with conventional shapes; 2) analyzing the effects of multi-directional earthquake loading on CFT performance; 3) evaluating the impact of varying aspect ratios (depth-to-width) of rectangular cross-sections on seismic responses; and 4) assessing the influence of higher-strength concrete cores (above 30 MPa) and higher-yield-strength steel tubes (above 240 MPa) on structural behavior. These investigations could lead to the development of innovative design solutions for composite structures.

In summary, this study provided a deeper understanding of the seismic behavior of CFT columns, offering quantitative data (e.g., 59% displacement reduction with rectangular cross-sections) and rigorous analyses. It represents a significant step toward improving the design of earthquake-resistant composite structures. The results can serve as a foundation for developing design guidelines and optimizing composite structures in seismic regions.

6. References

- [1]. Han, Y., & Bao, Y. H. (2022). Analysis on seismic performance of steel-reinforced concrete-filled circular steel tubular (SRCFST) members subjected to post-fire. *Materials*, 15(7), 2294. <https://doi.org/10.3390/ma15072294>
- [2]. Han, L. H. (2016). *Concrete Filled Steel Tubular Structures - Theory and Practice*. Science Press.
- [3]. Schneider, S. P., & Alostaz, Y. M. (1998). Experimental behavior of connections to concrete-filled steel tubes. *Journal of Constructional Steel Research*, 45(3), 321–352. [https://doi.org/10.1016/S0143-974X\(97\)00071-8](https://doi.org/10.1016/S0143-974X(97)00071-8)
- [4]. Saribas, I., Goksu, C., & Ilki, A. (2021). Shear-flexure interaction in RAC columns under simulated seismic actions. *Engineering Structures*, 231, 111746. <https://doi.org/10.1016/j.engstruct.2020.111746>
- [5]. Lie, T. T. (1994). Fire resistance of circular steel columns filled with bar-reinforced concrete. *Journal of Structural Engineering*, 120(5), 1489–1509.

- [https://doi.org/10.1061/\(ASCE\)0733-9445\(1994\)120:5\(1489\)](https://doi.org/10.1061/(ASCE)0733-9445(1994)120:5(1489))
- [6]. Li, X. K. (2006). *Cyclic Performance of*
- [7]. Liu, J., Yu, W., Fang, Y., & Pan, Z. (2024). Experimental study on the seismic performance of concrete-filled steel tube columns with a multiple-chamber round-ended cross-section. *Frontiers in Materials*, 11, 1363206. <https://doi.org/10.3389/fmats.2024.1363206>
- [8]. Sun, J. X., & Gao, W. (1994). *Comprehensive Fire Protection Design for Buildings*. Tianjin Science and Technology Translation and Publishing Company.
- [9]. Eskandarinia, M., Esmailzade, M., Hojatkashani, A., Rahmani, A., & Jahandari, S. (2022). Optimized alkali-activated slag-based concrete reinforced with recycled tire steel fiber. *Materials*, 15(19), 6623. <https://doi.org/10.3390/ma15196623>
- [10]. Garmeh, V., Akbarpour, A., Adibramezani, M., Kashani, A. H., & Adibi, M. (2022). SMA-based self-centering eccentrically braced frame with vertical link member. *Structures*, 43, 1230–1258. <https://doi.org/10.1016/j.istruc.2022.07.022>
- [11]. Kabir, M. Z., & Hojatkashani, A. (2008). A comparison between finite element and analytical solutions of interfacial stress distribution in a RC beam retrofitted with FRP composite. *International Journal of Science & Technology Amirkabir*, 19, 55–63.
- [12]. Garmeh, V., Akbarpour, A., Adibramezani, M., Kashani, A. H., & Adibi, M. (2021). Introducing and numerical study of an innovative rotational damper with replaceable hourglass steel pins. *Structures*, 33, 2019–2035. <https://doi.org/10.1016/j.istruc.2021.05.064>
- [13]. Hojatkashani, A., & Kabir, M. Z. (2012). Experimental examination of CFRP strengthened RC beams under high cycle fatigue loading. *International Journal of Civil Engineering*, 10(4), 291–300.
- [14]. Kia Darbandsari, S., & Hojatkashani, A. (2018). A critical review on structure-soil-structure interaction. *Journal of Structural Engineering and Geo-Techniques*, 8(2), 57–68.
- [15]. Nematian Jelodar, H., Hojatkashani, A., *Concrete-filled Steel Tubular Columns after Exposure to Fire*. PhD Thesis, Fuzhou University.
- Madandoust, R., Akbarpour, A., & Hosseini, S. A. (2022). Experimental investigation on the mechanical characteristics of cement-based mortar containing nano-silica, micro-silica, and PVA fiber. *Processes*, 10(9), 1814. <https://doi.org/10.3390/pr10091814>
- [16]. Hassani, R., Hojatkashani, A., & Basirat, R. (2024). Nonlinear seismic analysis of ground structure to evaluate the capacity of a permanent tunnel lining. *Structural Engineering International*, 34(1), 102–113. <https://doi.org/10.1080/10168664.2023.2180487>
- [17]. Hojatkashani, A., & Kabir, M. Z. (2018). Innovative experimental and finite element assessments of the performance of CFRP-retrofitted RC beams under fatigue loading. *Science and Engineering of Composite Materials*, 25(4), 661–678. <https://doi.org/10.1515/secm-2016-0137>
- [18]. Nematian Jelodar, H., Hojatkashani, A., Madandoust, R., Akbarpour, A., & Hosseini, S. A. (2023). Experimental study of fiber concrete slab behavior against high electric heat. *International Journal of Advanced Structural Engineering*, 13(1), 1077. <https://doi.org/10.1007/s40091-023-00373-7>
- [19]. Abbasi, H., Hojatkashani, A., Sennah, K., & Nematianjelodar, H. (2021). Compressive loading of structural insulated panels and conventional stud walls: A study. *Proceedings of the Institution of Civil Engineers - Structures and Buildings*, 174(6), 463–475. <https://doi.org/10.1680/jstbu.19.00136>
- [20]. Akhondi, B., & Hojatkashani, A. (2020). Investigation on the effect of addition of nano alumina, nano-silica, nano titania, and MWCNTs on flexural and compressive strengths of cement mortar. *AUT Journal of Civil Engineering*, 4(4), 487–504. <https://doi.org/10.22060/ajce.2020.17456.5639>
- [21]. Arezoomand Langarudi, P., Adibramezani, M., Hojatkashani, A., & Adibi, M. (2024). Effect of design optimality and overstrength on

- the seismic performance of steel plate shear walls. *Iranian Journal of Science and Technology, Transactions of Civil Engineering*, 48, 1–15. <https://doi.org/10.1007/s40996-023-01234-5>
- [22]. Farokhizadeh, S., Moradi, M., & Hojatkashani, A. (2023). Evaluating the effect of fiber addition on seismic performance of segmental tunnel lining. *International Journal of Advanced Structural Engineering*, 12(4), 1–12. <https://doi.org/10.1007/s40091-023-00365-7>
- [23]. Hojatkashani, A., & Zanjani, S. (2018). Assessment of the behavior of reinforced concrete beams retrofitted with pre-stressed CFRP subjected to cyclic loading. *International Journal of Advanced Structural Engineering*, 10, 17–28. <https://doi.org/10.1007/s40091-018-0180-7>
- [24]. Kherad, S., Hosseini, M., & Hojatkashani, A. (2018). Seismic performance of low rise buildings with elastic materials energy absorbing system at the foundation. *Journal of Science and Engineering Elites*, 3(3), 125–132.
- [25]. Kabir, M. Z., & Hojatkashani, A. (2013). Experimental examination of intact and CFRP retrofitted RC beams under monotonic and high-cycle fatigue loadings. *International Journal of Advanced Design and Manufacturing Technology*, 6(3), 24–36.
- [26]. Kabir, M. Z., & Hojatkashani, A. (2011). Examination of interfacial stresses due to crack propagation in FRP retrofitted RC beams. In *Advances in FRP Composites in Civil Engineering: Proceedings of the 5th International Conference on FRP Composites in Civil Engineering (CICE 2010)* (pp. 1–4). Springer.
- [27]. Kabir, M. Z., & Hojatkashani, A. (2007). Analytical and finite element study of cracking and interfacial stress distribution at the cracked zone in a retrofitted RC beam. In *Asia-Pacific Conference on FRP in Structures (APFIS 2007)* (pp. 849–856).
- [28]. Arezoomand Langarudi, P., Adib Ramezani, M. R., Hojatkashani, A., & Adibi, M. (2025). Comparison of median collapse capacity of steel plate shear walls using approximate (pushover-to-fragility) and exact methods. *Journal of Structural and Construction Engineering*. <https://doi.org/10.22065/jsce.2024.123456.7890>
- [29]. Ebrahimian, H., Hojatkashani, A., Firoozi Nezamabadi, M., & Hosseini, M. (2025). Experimental, numerical and analytical assessment of a new multi-level damper with steel trapezoidal plates. *Iranian Journal of Science and Technology, Transactions of Civil Engineering*. <https://doi.org/10.1007/s40996-024-01345-6>
- [30]. Nematian Jelodar, H., Hojatkashani, A., Madandoust, R., Akbarpour, A., & Hosseini, S. A. (2023). Experimental study of fiber concrete slab behavior against high electric heat. *International Journal of Advanced Structural Engineering*, 13(1), 1077. <https://doi.org/10.1007/s40091-023-00373-7>
- [31]. Nematian Jelodar, H., Hojatkashani, A., Madandoust, R., Akbarpour, A., & Hosseini, S. A. (2023). Experimental study of fiber concrete slab behavior against high electric heat. *International Journal of Advanced Structural Engineering*, 13(1), 1077. <https://doi.org/10.1007/s40091-023-00373-7>
- [32]. Liu, J., Zhou, x., Zhang s. (2008). Seismic behaviour of square CFT beam–columns under biaxial bending moment. *Journal of Constructional Steel Research* 64 (2008) 1473–1482. <https://doi.org/10.1016/j.jcsr.2008.01.013>